Communications Physics

https://doi.org/10.1038/s42005-026-02523-9

Article in Press

Network hierarchy entropy for quantifying graph dissimilarity

Received: 28 April 2025

Accepted: 22 January 2026

Cite this article as: Mou, J., Wang, L., Zhang, C. *et al.* Network hierarchy entropy for quantifying graph dissimilarity. *Commun Phys* (2026). https://doi.org/10.1038/s42005-026-02523-9

Jianhong Mou, Longyun Wang, Chaojun Zhang, Wenguan Luo, Suoyi Tan, Bin Zhou & Xin Lu

Network Hierarchy Entropy for Quantifying Graph Dissimilarity

Jianhong Mou[1], Longyun Wang[1], Chaojun Zhang[1], Wenguan Luo[1], Suoyi Tan[1], Bin Zhou[2], Xin Lu[1, *]

1. College of Systems Engineering, National University of Defense Technology, Changsha, 410073, China.
2. School of Management Science and Engineering, Nanjing University of Information Science and Technology, Nanjing, 210044, China.

[*] Corresponding author:

Xin Lu, College of Systems Engineering, National University of Defense Technology, Changsha, 410073, China, E-mail: xin.lu.lab@outlook.com.

Abstract

Quantifying subtle structural differences between networks remains a critical challenge across diverse scientific disciplines. Traditional network comparison methods often overlook the crucial role of edges and their interactions with nodes, thereby limiting their ability to capture complex structural dissimilarity governed by node-edge interplay. Here, we introduce a dissimilarity measure based on network hierarchy entropy, defined via the cross-entropy between node-level and edge-level distance distributions. This measure captures multiscale structural complexity by integrating hierarchical information encoded in shortest-path distributions across nodes and edges. Extensive experiments on synthetic and empirical networks show that this measure effectively discriminates fine-grained variations between networks with identical mesoscopic structures and robustly tracks evolving topologies in dynamic networks. It achieves 74.62% classification accuracy in distinguishing enzyme from non-enzyme proteins, comparable to state-of-the-art supervised learning models but without requiring feature engineering.

Introduction

Complex networks are pervasive across various domains, including biological structures[1], physical systems[2,3], and social network analysis[4,5]. Network dissimilarity and distance measures play a crucial role in analyzing shared information among multiple graphs[6-9]. For instance, in biology, comparing protein interaction networks across different human tissues can reveal both common and specialized mechanisms[10,11]. Similarly, in the social sciences, examining collaboration networks over time or across disciplines can uncover patterns of knowledge dynamics[12]. Many graph-level analytical tasks, such as network population clustering[10], regression[13,14], and classification[15,16], are highly sensitive to network dissimilarity measures. This sensitivity underscores the need for a detailed characterization of network topology and solutions capable of distinguishing subtle structural differences among networks[17-20], particularly when networks exhibit similar high-order structures[21].

Graph isomorphism and size invariance are critical challenges in network comparison[17,22]. Existing measures primarily focus on comparing descriptors derived from either the aggregate statistical properties of graphs[23-28] or their intrinsic spectral properties[29-33]. Recently, node distance-based approaches[34,35] have been developed and extended to measure the dissimilarity of weighted[36] and temporal networks[37], leveraging their advantages in recognizing isomorphic graphs and comparing networks with various sizes. Beyond these heuristic graph descriptors, graph neural networks[38-42] have been widely applied in network comparison for their superiority in feature embedding. However, most size-invariant network comparison methods predominantly emphasize node-level information and lack an explicit description of edge characteristics[43-45], thereby providing limited insight into the topological properties and structural roles of edges. The demonstrated efficacy of edge-centric approaches[46-48], such as line graphs and path neural networks, in tasks like node classification highlights the potential of incorporating edge features to better characterize network structure. Therefore, it is essential to quantify the criticality of edges in shaping networks from alternative perspectives and to characterize networks by integrating both node- and edge-level information.

Node and edge information are typically integrated into a unified latent feature space through embedding and convolutional operations[49-51]. While effective for tasks such as link prediction[50] and node classification[52], these approaches often treat node and edge features independently, overlooking their interdependencies. In network comparison, vector similarity measures[53] assess

dissimilarity by evaluating an edge's relative importance to its connected nodes through adjacency matrix transformations linked to node centrality. However, this reliance on node centrality can result in a primarily local perspective. Consequently, integrating node and edge structural information from a global viewpoint—emphasizing their interplay—would better capture edge topological features and provide a more comprehensive framework for analyzing network structures, thereby offering enhanced potential for detecting subtle network differences.

In this study, we investigate edge characterization through node pair shrinking and node-edge interplay using network hierarchy entropy (NHE) to quantify network dissimilarity. We apply our proposed measure to networks constructed to preserve identical distance distributions, thereby imposing stringent constraints on topological structure, to demonstrate its effectiveness in detecting subtle topological variations. Moreover, the metric exhibits high sensitivity to topological perturbations and demonstrates its utility across diverse applications, including evolving pattern analysis and protein classification.

Results

Network hierarchy entropy characterization

The hierarchy structure of node *i* describes the distribution of reachable nodes via shortest paths extending *l* steps away, denoted as, $\vec{\mathbf{S}}^{\boldsymbol{i}} = \frac{1}{N}(n_0^i, n_1^i, \dots, n_{L_i}^i)$, where L_i is the maximum length of shortest paths from node *i*, and n_l^i represents the number of nodes within layer *l*. Each layer *l* comprises the set of nodes at a distance *l* from the reference node. However, $\vec{\mathbf{S}}^{\boldsymbol{i}}$ captures only node-level reachability and omits edge-level information; consequently, identical $\vec{\mathbf{S}}^{\boldsymbol{i}}$ can correspond to structurally distinct networks, such as the Desargues and Dodecahedral graphs (see Fig.1 (a)). To differentiate such networks, we examine edge features and observe that differing connections between consecutive hierarchical layers produce varying sets of nodes that are simultaneously two steps from node *j* and three steps from node *i*. Put differently, the count of nodes closer to node *j* than to node *i* differs across these networks. This pattern reflects distinct properties of the edge e_{ij}, arising from the interdependence between its connected nodes, and can be captured through node pair shrinking, which merges the two nodes into a new node connecting to their combined neighbors (see Fig.1 (a)). The hierarchy structure of the new node is defined as the edge hierarchy structure, i.e., $\vec{\mathbf{S}}^{\boldsymbol{e_{ij}}} = \frac{1}{N-1}(n_0^{e_{ij}}, n_1^{e_{ij}}, \dots, n_{L_{ij}}^{e_{ij}})$. Fundamentally, the edge

hierarchy structure characterizes the relationship between the distance from any node k to the merged node and its distance to the original endpoints i and j, yielding $d_{k,e_{ij}} = \min(d_{k,i}, d_{k,j})$. Specifically, in the context of network spreading, it indicates the possible propagation paths by simultaneously infecting node pairs.

Hierarchical structure is fundamentally linked to network spreading[54-56], as diffusion generally propagates from the origin node to its immediate neighbors, then to second-order neighbors, continuing outward until reaching the maximum neighborhood. To capture this progression, we integrate hierarchy structure by weighting nodes according to their distance from the source and propose node hierarchy centrality (NHC) and edge hierarchy centrality (EHC):

$$C_v^i = \frac{1}{N}\sum_{l=0}^{L_i}\frac{n_l^i}{l!} \quad (1)$$

$$C_e^{ij} = \frac{1}{N-1}\sum_{l=0}^{L_{ij}}\frac{n_l^{e_{ij}}}{l!} \quad (2)$$

The factorial weight $l!$ provides a unique characterization of node and edge hierarchy structures, eliminating potential ambiguities that arise from the specific ordering of elements in the hierarchy vector. Furthermore, the explicit inclusion of the layer l=0 is essential for accurately quantifying the spreading process, as it represents the initial seed of infection (see Supplementary Note 1). To evaluate the efficiency of hierarchy centrality in identifying influential spreading nodes and edges, we benchmarked the spreading influence by the average outbreak size[57-59], defined as the sum of infected and recovered individuals resulting from initially infecting a single node or edge. This assessment is conducted through 1,000 independent simulations of the susceptible-infected-recovered (SIR) model[60]. The high Kendall's τ values between node (edge) rankings based on NHC (EHC) and the spreading influence on 14 empirical networks illustrate the outperformance of hierarchy centrality in identifying key nodes and edges compared to 6 traditional node and edge centralities (see Fig.1 (b)).

Although edge hierarchy centrality facilitates the comparative analysis of specific graphs like the Desargues and Dodecahedral structures, its broader applicability to diverse network architectures is constrained. This limitation is evidenced by the failure of average node and edge hierarchy centralities to reliably discriminate not only between simple toy networks perturbed by a single edge removal (see Supplementary Fig. S5) but also between non-isomorphic networks derived from the Chemical network that share identical distance distributions up to distance 8 (see Supplementary Fig. S6).

The following foundational metric, which defines the distance from any node k to an edge e_{ij} in relation to the distances from k to its endpoints i and j, provides an efficient framework for quantifying hierarchical relationships between nodes and edges. Given that hierarchy centrality effectively characterizes node and edge hierarchy structure, we introduce network hierarchy entropy to precisely measure the interaction between a node or edge and its local neighborhood based on their NHC and EHC. Specifically, edge hierarchy entropy (EHE) captures the divergence between the EHC distribution and the average NHC of its incident nodes. This entropy thus quantifies the information loss incurred when the edge hierarchy centrality is approximated by the mean hierarchy centrality of its endpoints. Analogously, node hierarchy entropy (NHE) measures the divergence between the NHC distribution and the average EHC of its incident edges (see Fig.1 (c)), revealing the information loss when the node centrality is approximated by the average centrality of its connected edges. To ensure that these hierarchy entropies are size invariant, they are divided by the number of edges (M) and nodes (N), respectively:

$$T_{\mathrm{EHE}} = \frac{-\sum_{ij} c_e^{ij} \log \frac{(c_v^i + c_v^j)}{2}}{M} \tag{3}$$

$$T_{\mathrm{NHE}} = \frac{-\sum_k c_v^k \log \frac{\sum_{l \in N_k} c_e^{kl}}{|N_k|}}{N} \tag{4}$$

Given that EHE and NHE quantify information loss from the perspective of hierarchy centrality which is established as a proxy for spreading influence, we evaluate their practical significance by correlating them with infection gains. We define the edge infection gain, ΔI_e, as the expected increase in outbreak size from simultaneously infecting both endpoints of an edge versus targeting them individually. Analogously, the node infection gain, ΔI_k, measures the potential increase in infections achieved by targeting one of the neighbors collectively rather than the central node itself. Our analysis of the Faa network reveals a strong correlation between hierarchy entropy and infection gains. Furthermore, nodes and edges with low entropy are predominantly located at the network periphery (see Fig. 1(d)).

NHE-based network dissimilarity

Network dissimilarity or network distance quantifies the structural difference between two graphs. This is typically achieved by mapping the graphs to a feature space and measuring the distance between their corresponding representations. In this work, we define the dissimilarity

between two networks g_1 and g_2 as the Euclidean distance between their corresponding T_{NHE} and T_{EHE} values:

$$d_{\mathrm{NHE}} = \sqrt{(T_{\mathrm{NHE}}^{\mathrm{g1}} - T_{\mathrm{NHE}}^{\mathrm{g2}})^2 + (T_{\mathrm{EHE}}^{\mathrm{g1}} - T_{\mathrm{EHE}}^{\mathrm{g2}})^2} \quad (5)$$

This measure satisfies fundamental mathematical properties, namely reflexivity, symmetry, and the triangle inequality, thereby constituting a valid metric. Furthermore, it adheres to key intuitive principles, including edge importance and edge submodularity[33] (see Supplementary Fig. S7). The edge importance principle posits that modifications that create disconnected components should incur a greater penalty than those that preserve connectivity. The edge submodularity principle states that the impact of an edge alteration is more pronounced in a sparse graph than in a denser graph of the same size.

The proposed dissimilarity measure reveals distinctive features in simple networks (see Supplementary Note 2). Specifically, the homogeneity of nodes and edges in complete networks results in $T_{\mathrm{NHE}} = T_{\mathrm{EHE}} = 0$, leading to $d_{\mathrm{NHE}} = 0$ when comparing complete networks of different sizes. This observation aligns with the use of complete networks as null models for assessing spreading capacity[61]. For star networks, the entropy values $T_{\mathrm{NHE}} = 0$ and $T_{\mathrm{EHE}} = \log(\frac{3}{4} + \frac{1}{2n})$ indicate increasing similarity among star networks as their size grows. In line and cycle networks, besides showing increasing similarity between networks of comparable sizes, the measure also reflects convergence toward the properties of networks of their original size. This pattern is supported by the theoretical upper bound of NHE and EHE, where T_{NHE} has been proven to remain below 1/e, alongside the convergence of entropy values toward those observed in the initial configurations.

The computational complexity of the proposed algorithm is dominated by the construction of hierarchical structures for all nodes and edges. This process is achieved by performing a Breadth-First Search (BFS) from every node to compute its shortest-path distance distribution. The hierarchy for any edge e_{ij} is then derived efficiently from the precomputed distributions of its endpoints, using the relation $d_{k,e_{ij}} = \min(d_{k,i}, d_{k,j})$. This approach avoids the cost of performing additional BFS computations for each edge. Consequently, the total time complexity is $O(N(M + N))$, governed by the N BFS operations over the graph (see Supplementary Note 3). The pseudocode of network hierarchy entropy-based dissimilarity is illustrated in Supplementary Algorithm 1.

Characterizing the topological features of synthetic networks

To evaluate the discriminative power of network similarity measures, we quantified pairwise distances among synthetic networks, including Watts-Strogatz (WS), Erdős-Rényi (ER), Barabási–Albert (BA), and Lancichinetti-Fortunato-Radicchi (LFR) networks generated under varying parameters with 5 realizations for each parameter (see Supplementary Table S3). From this section onward, we examine the efficiency of NHE compared to 5 size-invariant network heuristic dissimilarity metrics inspired by matrix distances, graph statistics, spectral distances, and hybrid measures, including Portrait divergence (POR)[25], NetSimile measure[24], Ipsen–Mikhailov distance (IM)[62], NetLSD measure[32], and D-measure[34].

In the coarse-grained task of classifying networks solely by their generative model, all evaluated metrics performed poorly, achieving a normalized mutual information (NMI) score below 0.52 under classical hierarchical clustering with a complete-linkage criterion. In contrast, for the fine-grained clustering of networks into 24 categories based on specific parameters, NHE achieves a high NMI of 0.808, while NetSimile yields the highest performance with an NMI of 0.912 (see Fig.2 and Supplementary Table S4). Beyond clustering performance, NHE also exhibits a strength in identifying and elucidating the intrinsic evolutionary patterns inherent to each generative model. Alongside the IM and NetLSD metrics, NHE successfully identifies key topological transitions, including the transition of the small-world structure in WS networks at a critical rewiring probability p_r=0.1, the percolation transition in ER networks at the critical connecting probability p_c=0.001, and the emergence of cycles in BA networks with m>1 (see Supplementary Fig. S8). In addition, NHE assigns small dissimilarity values among LFR networks with a strong community structure (mixing parameter μ = 0.1), while identifying large distances between these and LFR networks with weaker community organization (μ = 0.2, 0.3, 0.4). This pattern is absent in other competing methods. Collectively, these results underscore that different metrics can reveal complementary aspects of network structure.

NHE captures finer structural details of networks

Networks that share a greater number of structural properties exhibit lower pairwise dissimilarity. We extend the effectiveness of the proposed method to empirical networks using the dk series model[21]. This model generates randomized networks that sequentially preserve an increasing number of key structural properties, including degree correlation (dk2.0), average clustering (dk2.1), and degree-dependent clustering (dk2.5). Consequently, a higher k-parameter

captures more structural information from the original network, which in turn should yield a lower measured dissimilarity to the original network.

Analysis of the average distance over 50 randomized realizations between each *dk*-series model and its original network (see Fig. 3 (a)) reveals that IM and POR significantly blur the distances among *dk*-series models and the original network across six and two networks, respectively. This finding contradicts the established principle that models with higher *k*-values retain more structural information from the original network and should, therefore, exhibit smaller distances to it. Specifically, IM and POR fail to distinguish the descriptive capabilities of dk2.0 and dk2.1 for the Technology network. This expected ordinal relationship is visually confirmed by the LaNet-vi graphic layout[63] (see Fig. 3 (b)), which is widely used for visually comparing topological differences among networks[21]. In contrast, NHE and NetLSD exhibit significant deviations in only one network, whereas NetSimile shows non-significant deviations in one network and D-measure in three networks. The statistical significance of these results is supported by a paired t-test (see Supplementary Fig.S9 and Supplementary Table S5-S7 for details).

Although NHE does not yield the most significant gradation across the dk-series, it demonstrates exceptional performance in clustering randomized samples generated from the same dk model. As summarized in Table 1 and Supplementary Fig. S10, NHE achieves superior performance in dk-series network classification, attaining the highest normalized mutual information (NMI) score for 10 out of the 14 networks tested. Perfect clustering (NMI = 1.0) is achieved for 9 of these networks. A key finding is that NHE is the sole metric capable of correctly clustering the dk-series realizations for the Web network.

Comparing networks preserving the node hierarchy structure

NHE is primarily designed to address the limitations of node hierarchy structure in characterizing network topology, particularly since many networks may exhibit the same hierarchy due to a lack of consideration for connecting details. To validate the superiority of the proposed method in detecting subtle variation among networks with several identical topological statistics, we introduce a simulated annealing algorithm[64,65] that generates a network assembly preserving the node hierarchy structure (see *Methods*). Specifically, we initialize random networks that maintain the degree distribution, and then we randomly select pairs of edges for reconfiguration if doing so either decreases the system's energy or meets the probabilistic acceptance criterion. The energy is defined as the distance between the node hierarchy structures

of the original and randomized networks. Simulated annealing effectively navigates the solution space, preventing the search from becoming trapped in local minima (see Fig.4 (a-b)).

The node hierarchy structure has been explicitly demonstrated to relate to various topological statistics, including degree distribution, average shortest path length, node betweenness, and edge betweenness[55]. The dissimilarity of networks within this type of assembly is primarily attributed to high-level structures, such as subgraphs and the number of shortest paths (see Fig.4 (c)). The evaluation of dissimilarity metrics hinges on two aspects, including the ability to distinguish networks that preserve the same structural properties as a reference network, and their performance in classifying networks. From the perspective of network discrimination, both POR and the D-measure struggle to differentiate hierarchy-preserving variants of the Karate[66], Polbooks, and Synapse networks (see Fig. 4 and Supplementary Fig. S11–S13), yielding average pairwise distances that are either zero or nearly zero among networks that maintain identical hierarchical structure. Although effective for quantifying general structural dissimilarity (e.g., in the Karate network), NetSimile fails to distinguish networks with identical topological statistics, a limitation inherent to its design. We demonstrate this by generating an ensemble of networks from the Chemical network using the simulated annealing method, as well as networks preserving degree correlations of the London network. In contrast, NetLSD, IM, and NHE successfully resolve these structurally similar instances. From the network classification perspective, IM obscures the distinction between distances within degree-preserving networks and those between degree-preserving and hierarchy structure-preserving networks, reporting similar average intra- and inter-class distances of 0.131 and 0.138, respectively (see Fig.4 (d)). All other methods maintain a clear separation in this task. Collectively, only NetLSD and NHE demonstrate consistent effectiveness in both distinguishing and classifying networks that preserve node hierarchy structure, underscoring their sensitivity to topological variation.

Evolving pattern characterization for temporal networks

To evaluate the effectiveness of network hierarchy entropy in detecting changes within dynamic systems, we applied it to characterize the evolving pattern for mobility behaviors during the spread of COVID-19 from January 1st to February 29th, 2020. This period encompasses regular travel, the Lunar New Year travel season (Chunyun), population flow restriction, and the subsequent recovery phases. We quantify the distance between mobility networks among 367 cities, using the network on January 1st as a baseline, assuming that mobility behavior before

Chunyun represents normal conditions without critical disturbances. The results demonstrate that NHE effectively captures variations in mobility networks, strongly supported by the temporal changes in spatial communities and other classical topological features (see Fig.5 (a-c)). In contrast, NetLSD and POR fail to capture the evolving mobility patterns. Furthermore, the D-measure incorrectly quantifies the dissimilarity between networks from the normal mobility phase and the onset of quarantine (i.e., January 23rd), as evidenced by anomalously short distances (see Fig. 5(d)). The efficacy of NHE is further demonstrated through two distinct analytical approaches: (1) a stepwise analysis, which compares each network snapshot only to the prior one, and (2) a comprehensive analysis, which compares every snapshot to all others (see Supplementary Note 4). Specifically, both NHE, IM, and NetSimile effectively facilitate the identification of critical topological perturbations. However, IM and NetSimile erroneously cluster snapshots from before January 10th (a period of normal mobility) with those from slightly after January 23rd (the strict quarantine phase).

Distinguishing enzyme structures from non-enzymes for proteins

The intrinsic relationship between protein structure and function allows for functional differentiation based on the topological dissimilarity of protein networks. By quantifying these topological differences, we can group proteins with similar structural and functional characteristics. To achieve this, we employ a classical hierarchical clustering with a complete-linkage criterion, applied to the matrix of pairwise topological distances between networks, to classify proteins into functionally relevant groups. Results indicate that the NHE-based clustering method achieves an accuracy of 74.62% and an F1 score of 64.11% (see Fig.6 and Supplementary Table S8), significantly outperforming competing methods and being comparable to most supervised neural network approaches[67], which report accuracies ranging from 76.15 ± 2.56% to 80.14 ± 4.38%. Furthermore, NHE demonstrates the highest valid clustering efficiency excluding the outlier NetLSD (see Fig.6 (a)), achieving a Silhouette coefficient[68] of s=0.606. This indicates its superior ability to minimize within-group distances while maximizing between-group distances, resulting in a meaningful and robust separation. In contrast, NetLSD attains a high but misleading coefficient (s=0.958). This artifact stems from the formation of a small, spurious cluster containing only two false-positive enzymes (TP=0, FP=2), which does not represent a biologically meaningful partition (see Supplementary Table S8). The significantly lower distribution of three- and four-node subgraph counts among identified enzymes, compared to non-enzymes, indicates that NHE

usually characterizes enzymes by their reduced participation in these interaction subgraphs (see Fig.6 (b)).

Discussion

Network hierarchy entropy (NHE) provides a highly precise measure for quantifying network dissimilarity by capturing the interactions of distance-based vectors among nodes and edges. Unlike line graph approaches, it characterizes edge criticality through node pair shrinking. This technique quantifies the interaction between two endpoint nodes by considering the minimal distance from any node to the merged pair. In the context of network spreading, this operation fundamentally models the potential gain in outbreak size achieved by simultaneously infecting both endpoints, rather than targeting a single node. The hierarchy centrality component of this measure is strongly correlated with network spreading dynamics and effectively identifies influential spreaders. Meanwhile, the cross-entropy component quantifies information loss when node or edge distance distributions are approximated by those of neighboring edges or nodes, closely relating to infection gains from infecting node pairs simultaneously. Through extensive experiments, we demonstrate that NHE accurately detects subtle topological variations and high-order dissimilarities between networks. Additionally, it outperforms alternative methods in detecting evolving patterns in dynamic systems and in distinguishing enzyme structures from non-enzymes.

Node pair shrinking effectively captures nodes that are l steps away from one node and $l + 1$ steps away from its connected counterpart. This concept extends the classical notion of common neighbors and shows promise for tasks involving node correlation, such as node similarity characterization and link prediction. The hierarchy centrality-based cross-entropy quantifies the information gain arising from the combinational effect, particularly in network spreading, thereby aiding the identification of critical diffusion paths. The impact of these paths on network dynamics warrants further investigation, especially in scenarios that slow spreading while preserving overall connectivity[69].

One critical challenge arises from using the simulated annealing algorithm to preserve node hierarchy structures in sparse graphs, as these graphs typically produce relatively long node hierarchy vectors. Such vectors impose stricter topological constraints, complicating the search for an optimal solution. Furthermore, the reconstructability of networks with varying node hierarchy structures enables a more comprehensive understanding of how distance, rather than degree

distribution[70], influences network topology. Importantly, because node hierarchy structures are strongly associated with the network correlation dimension[54,71,72], a metric that provides more accurate predictions of early spreading, identifying networks with similar propagation dynamics will facilitate deeper insights into the interplay between topology and function.

While node and edge hierarchy entropies effectively classify synthetic networks with diverse community structures, a promising direction for future research is to explore how network hierarchy and hierarchy entropy can be leveraged for community detection. Moreover, integrating edge and node–edge interactions could enable the analysis of weighted, directed, multilayer, and temporal networks, thereby expanding their applicability in both structural and functional studies. These advancements would significantly deepen our understanding of complex networks from a more comprehensive and nuanced perspective.

Methods

Network data

Synthetic networks We choose generative network models that are common and reflect several topological properties of real-world networks, including ER, WS, BA, and LFR networks (see Supplementary Table S3).

ER model[73] constructs networks by connecting each pair of nodes with probability p_c. As p_c increases, the model exhibits a phase transition from a fragmented state, consisting of many small, disconnected components, to a fully connected network.

WS model[74] explains the coexistence of a high clustering coefficient and a short distance (small-world behavior) by rewiring links with probability p_r in a ring lattice with non-overlap connections to K nearest neighbors for each node. This construction allows us to tune the graph between a symmetric state with long distances ($p_r = 0$) and a disordered state with short distances ($p_r = 1$).

BA model[75] generates random scale-free networks using a preferential attachment mechanism. It aims to explain the existence of highly heterogeneous degree distribution in real networks. It generates a graph by attaching new nodes along with m edges, which are attached to existing nodes in proportion to their degree.

LFR model[76] excels at generating networks with predefined community structures, degree distributions, and mixing patterns. By creating communities of diverse sizes and varying levels of inter-community connectivity, LFR networks realistically mimic the complex topology observed in real-world systems. We synthesized multiple LFR networks varying in degree distribution exponent (λ), and community structure parameter (μ).

General empirical networks We utilize 14 empirical networks to examine the correlation between hierarchy centrality and network spreading, to assess the efficiency of network hierarchy entropy in quantifying dissimilarity. For consistency, self-loops, directionality, and edge weights are removed, and only the giant connected components of the networks are considered. Detailed information about these networks is provided in Supplementary Note 5.

Temporal mobility network To extend the application of the proposed metric to evolving pattern detection, we analyze a temporal mobility network that captures physical mobility behaviors. This network represents mobility among 367 cities in China[77], constructed using nationwide mobile phone data collected between January 1st and February 29th, 2020. The dataset spans diverse periods, including normal travel from January 1st to 9th, the Lunar New Year travel season (a.k.a., Chunyun) from January 10th to 22nd, the population flow restrictions during COVID-19 quarantine measures from January 23rd to February 9th, and the subsequent recovery phase after February 10th. Directionality and edge weights are removed.

Biological macromolecule networks To evaluate the performance of the proposed metric in graph classification, we apply it to distinguish enzyme from non-enzyme proteins[78]. All macromolecule networks are undirected and unweighted. Specifically, this dataset includes 1,178 high-resolution protein structures extracted from a non-redundant subset of the protein database using simple features such as secondary structure content, amino acid propensity, surface properties, and ligands. In this representation, nodes correspond to amino acids, and an edge is drawn between two nodes if the distance between them is less than six angstroms. The dataset is divided into two functional categories: 487 enzymes and 691 non-enzymes.

SIR model

Given the strong relationship between hierarchy and network spreading, we evaluate the effectiveness of NHC and EHC in identifying influential spreaders. The ground-truth spreading influence of each node and edge is quantified by the average outbreak size, namely the total

number of infected and recovered individuals, over 1,000 independent Susceptible-Infected-Recovered (SIR) simulations[53]. The spreading process evolves through contacts between infected and susceptible nodes with probability β, while infected nodes recover with probability γ. The recovery rate in the SIR model is fixed at γ=1, while the infection rate β ranges from $0.2\beta_c$ to $1.8\beta_c$, where $\beta_c = \frac{\langle k \rangle}{\langle k^2 \rangle - \langle k \rangle}$[55-58]. For edges, propagation dynamics are modeled by the simultaneous infection of both connected nodes.

Simulated annealing algorithm

Simulated annealing[64,65] is an optimization algorithm designed to approximate the global minimum of a given cost function, with a temperature parameter T controlling its progression. At high temperatures, the algorithm explores the solution space broadly, enabling extensive configuration sampling. As the temperature decreases, the search becomes more focused, allowing only small changes that minimally increase the system's cost. The process starts with a high initial temperature to avoid entrapment in local minima and gradually cools, guiding the system through the optimization landscape while restricting uphill moves. Here, the cost function H is minimized, which is defined as the total difference in node distance distributions between the original network and the randomized variants.

During the optimization process, networks preserving the original degree distribution are used as the initial configurations. Optimization proceeds by randomly swapping pairs of edges. A proposed reconfiguration is accepted if it reduces the system's cost function or satisfies the probabilistic Metropolis acceptance criterion, defined as $r < exp(-\Delta H/T)$, where r is a random number in [0,1]. The annealing schedule performs $100M$ edge swaps at each stage, with M denoting the total number of edges. The temperature is reduced progressively at a fixed rate of 0.95 per stage, i.e., $T_{i+1} = 0.95 \times T_i$. Importantly, the simulated annealing process does not impose any specific assumptions on the hierarchical properties of networks. System performance is evaluated at each stage, and the annealing terminates if and only if the energy reaches zero. Detailed pseudocode for the simulated annealing algorithm that preserves the node hierarchy structure is provided in Supplementary Algorithm 2.

Given the challenges posed by the strict constraints of node hierarchy in finding configurations where the energy reaches zero, we explore a non-monotonic annealing schedule that incorporates reheating to overcome local minima. While monotonic cooling usually helps the

system escape local minima, it can become trapped in low-temperature regimes when the cost of necessary rearrangements is too high. To address this, we enhance the simulated annealing algorithm with a reheating mechanism triggered upon detection of a local minimum where no accepted edge swaps occur over 20 consecutive annealing stages. At this point, the temperature is reset to half the initial value, i.e., $T_{i+1} = T_0/2$. This modification restores the system's exploratory ability, improving its chances of escaping unfavorable configurations.

Competing methods

Portrait divergence (POR)[25] quantifies network dissimilarity by measuring the distance between probability distributions that represent the number of nodes with *k* neighbors at distance *l*. Specifically, it constructs network portraits $\mathbf{B}_1$ and $\mathbf{B}_2$ for networks g_1 and g_2, encoding this information. These portraits are converted into distributions $\mathbf{P}_1$ and $\mathbf{P}_2$, which describe the probability of two randomly chosen nodes being connected at distance *l* and having *k* neighbors. The dissimilarity d_{POR} is then defined as the Jensen-Shannon divergence between $\mathbf{P}_1$ and $\mathbf{P}_2$.

NetSimile measure[24] compares networks by integrating descriptive and numerical features in three steps. First, it computes a predefined set of numerical features for each node, including node degree, clustering coefficient, average degree of neighborhood, average clustering coefficient of neighborhood, number of edges within the neighborhood, number of outgoing edges from the neighborhood, and number of neighbors of neighbors (not in the neighborhood). Second, these features are transformed into a "signature" vector containing aggregated statistics (e.g., median, mean, standard deviation, skewness, kurtosis). Finally, the measure $d_{\mathrm{NetSimile}}$ compares graphs concerning the Canberra Distance of "signature" vectors.

Ipsen–Mikhailov (IM) distance[62] leverages the spectral density of eigenvalues from the graph Laplacian to provide an invariant characterization of networks. It interprets a network with *N* nodes as a system of *N*-particle molecules connected by identical elastic strings, where vibration frequencies are described by the graph spectrum. The spectral density $\rho(\omega)$ is introduced as a sum of narrow Lorentz distributions. The IM distance d_{IM} is then defined as the difference between the spectral densities of networks.

NetLSD measure[32] extracts a compact signature based on the Laplacian spectrum of a graph, thereby hearing the shape of a graph. It computes the normalized Laplacian matrix $\mathbf{L} = \mathbf{I} - \mathbf{D}^{\frac{-1}{2}}\mathbf{A}\mathbf{D}^{\frac{-1}{2}}$ and models a heat diffusion process using the heat equation $v'(t) = -\mathbf{L}v(t)$. The

closed-form solution of this equation is given by the kernel matrix $H_t = e^{-t\mathbf{L}}$ that represents the amount of heat transferred among the nodes at time *t*. The NetLSD measure summarizes this information by computing heat traces $tr(H_t)$ at different time *t*. The dissimilarity d_{NetLSD} between graphs is then measured as the Frobenius norm of the difference between their heat trace vectors.

D-measure[34] is proposed by comparing the dissimilarity of networks concerning their network distance distributions, node distance distributions, and the analysis of α-centrality. The network distance distribution quantifies the heterogeneity of a graph in terms of connectivity distances. The D-measure $d_{\mathrm{D-measure}}$ between graphs g_1 and g_2 is calculated as the difference between their averaged node-distance distributions, as well as between the α-centrality values of the graphs and their complements.

Data Availability

All relevant data are available at https://github.com/JHMou/network-hierarchy-entropy-based-dissimilarity.

Code availability

Software for dk-series model is available at http:// polcolomer.github.io/RandNetGen/.
Other involved codes are available at https://github.com/JHMou/network-hierarchy-entropy-based-dissimilarity.

References

1 Liu, C. et al. Computational network biology: Data, models, and applications. *Phys. Rep*. **846**, 1–66 (2020).

2 Liu, Y., Dehmamy, N. & Barabasi, A.-L. Isotopy and energy of physical networks. *Nat. Phys.* **17**, 216–222 (2021).

3 Pete, G., Timár, A., Stefánsson, S. O., Bonamassa, I. & Pósfai, M. Physical networks as network-of-networks. *Nat. Commun.* **15**, 4882 (2024).

4 Meng, F. et al. Spreading dynamics of information on online social networks. *Proc. Natl Acad. Sci. USA* **122**, e2410227122 (2025).

5 Su, S., Dai, Y., Xu, X. & Zhong, Z. Competition or coexistence: Diffusion network differences between entertainment events and public events on social media. *Inf. Process. Manag.* **62**, 104087 (2025).

6 Barabási, A.-L., Gulbahce, N. & Loscalzo, J. Network medicine: a network-based approach to human disease. *Nat. Rev. Genet.* **12**, 56–68 (2010).

7 De Domenico, M., Nicosia, V., Arenas, A. & Latora, V. Structural reducibility of multilayer networks. *Nat. Commun.* **6**, 6864 (2015).

8 Menche, J. et al. Uncovering disease-disease relationships through the incomplete interactome. *Science* **347**, 1257601 (2015).

9 Taylor, D. et al. Topological data analysis of contagion maps for examining spreading processes on networks. *Nat. Commun.* **6**, 7723 (2015).

10 Coupette, C., Dalleiger, S. & Vreeken, J. Differentially describing groups of graphs. in *Proc. 36th AAAI Conf. Artif. Intell.* 3959–3967 (AAAI, 2022).

11 Huttlin, E. L. *et al.* Dual proteome-scale networks reveal cell-specific remodeling of the human interactome. *Cell* **184**, 3022-3040 (2021).

12 Ren, R. & He, J. Network traits driving knowledge evolution in open collaboration systems. *PloS one*. **18**, e0291097 (2023).

13 Hamilton, W. L., Ying, R. & Leskovec, J. Inductive representation learning on large graphs. in *Proc. Adv. Neural Inf. Process. Syst.* **30** 1025–1035 (2017).

14 Zhou, Y. & Müller, H.-G. Network regression with graph Laplacians. *J. Mach. Learn. Res.* **23**, 320 (2022).

15 Kipf, T. N. & Welling, M. Semi-supervised classification with graph convolutional networks. *Proceedings of the 2017 International Conference on Learning Representations* 1-14, (ICLR, 2017).

16 Lee, J. B., Kong, X., Moore, C. M. & Ahmed, N. Deep parametric model for discovering group-cohesive functional brain regions. in *Proc. SIAM Int. Conf. Data Mining* 631–639 (SIAM, 2020).

17 Hartle, H. et al. Network comparison and the within-ensemble graph distance. *Proc. R. Soc. A* **476**, 20190744 (2020).

18 Mao, S. & Zeng, X.-J. SimVGNets: Similarity-Based Visibility Graph Networks for Carbon Price Forecasting. *Expert Syst. Appl.* **230**, 120647 (2023).

19 Shvydun, S. Models of similarity in complex networks. *PeerJ Comput. Sci.* **9**, e1371 (2023).

20 Felippe, H., Battiston, F. & Kirkley, A. Network mutual information measures for graph similarity. *Commun. Phys* **7**, 1-12 (2024).

21 Orsini, C. et al. Quantifying randomness in real networks. *Nat. Commun.* **6**, 8627 (2015).

22 Wang, Y. & Zhang, M. An empirical study of realized GNN expressiveness. in *Proc. Int. Conf. Mach. Learn*. 52134–52155 (PMLR, 2024).

23 Zhou, B., He, Z., Wang, N. & Wang, B.-H. A method of characterizing network topology based on the breadth-first search tree. *Physica A* **450**, 682–686 (2016).

24 Berlingerio, M., Koutra, D., Eliassi-Rad, T. & Faloutsos, C. Network similarity via multiple social theories. in *Proceedings of the 2013 IEEE/ACM International Conference on Advances in Social Networks Analysis and Mining*. 1439–1440 (IEEE, 2013).

25 Bagrow, J. P. & Bollt, E. M. An information-theoretic, all-scales approach to comparing networks. *Appl. Netw. Sci.* **4**, 15 (2019).

26 Coupette, C. & Vreeken, J. Graph similarity description: how are these graphs similar? in *Proc. 27th ACM SIGKDD Conf. Knowl. Discov. Data Mining* 185–195 (ACM, 2021).

27 Carpi, L. C., Rosso, O. A., Saco, P. M. & Ravetti, M. G. Analyzing complex networks evolution through Information Theory quantifiers. *Phys. Lett. A* **375**, 801–804 (2011).

28 Chen, D., Shi, D., Qin, M., Xu, S. & Pan, G. Complex network comparison based on communicability sequence entropy. *Phys. Rev. E* **98**, 012319 (2018).

29 Mellor, A. & Grusovin, A. Graph comparison via the nonbacktracking spectrum. *Phys. Rev. E* **99**, 052309 (2019).

30 Torres, L., Suárez-Serrato, P. & Eliassi-Rad, T. Non-backtracking cycles: length spectrum theory and graph mining applications. *Appl. Netw. Sci.* **4**, 41 (2019).

31 Su, H. a. C., Dan and Pan, Gui-Jun and Zeng, Zhigang. Identification of Network Topology Variations Based on Spectral Entropy. *IEEE T. Cybern.* **52**, 10468-10478 (2022).

32 Tsitsulin, A. et al. NetLSD: hearing the shape of a graph. in *Proc. 24th ACM SIGKDD Int. Conf. Knowl. Discov. Data Mining* 2347–2356 (ACM, 2018).

33 Koutra, D., Shah, N., Vogelstein, J. T., Gallagher, B. & Faloutsos, C. DeltaCon: principled massive-graph similarity function with attribution. *ACM Trans. Knowl. Discov. Data* **10**, 28 (2016).

34 Schieber, T. A. et al. Quantification of network structural dissimilarities. *Nat. Commun.* **8**, 13928 (2017).

35 Zhang, Z. W. X.-X. Z. C. L. Z.-K. Quantification of network structural dissimilarities based on network embedding. *iScience* **25**, 104446 (2022).

36 Jiang, Y., Li, M., Fan, Y. & Di, Z. Characterizing dissimilarity of weighted networks. *Sci. Rep.* **11**, 5768 (2021).

37 Zhan, X.-X. et al. Measuring and utilizing temporal network dissimilarity. *Commun. Phys.* **8**, 40 (2025).

38 Bai, Y. et al. SimGNN: a neural network approach to fast graph similarity computation. in *Proc. 12th ACM Int. Conf. Web Search Data Mining* 184–192 (ACM, 2019).

39 Buterez, D., Janet, J. P., Kiddle, S. J., Oglic, D. & Lió, P. Transfer learning with graph neural networks for improved molecular property prediction in the multi-fidelity setting. *Nat. Commun.* **15**, 1517 (2024).

40 Li, Y. et al. Graph matching networks for learning the similarity of graph structured objects. in *Proc. Int. Conf. Mach. Learn.* 3835–3845 (PMLR, 2019).

41 Ma, G., Ahmed, N. K., Willke, T. L. & Yu, P. S. Deep graph similarity learning: a survey. *Data Min. Knowl. Discov.* **35**, 688–725 (2021).

42 Wan, Y., Yuan, C., Zhan, M. & Chen, L. Robust graph learning with graph convolutional network. *Inf. Process. Manag.* **59**, 102916 (2022).

43 Abu-Aisheh, Z., Raveaux, R., Ramel, J.-Y. & Martineau, P. A parallel graph edit distance algorithm. *Expert Syst. Appl.* **94**, 41–57 (2018).

44 Čech, P. Matching UML class models using graph edit distance. *Expert Syst. Appl.* **130**, 206–224 (2019).

45 Gao, X., Xiao, B., Tao, D. & Li, X. A survey of graph edit distance. *Pattern Anal. Appl.* **13**, 113–129 (2010).

46 Chen, Z., Li, L. & Bruna, J. Supervised community detection with line graph neural networks, *Proceedings of the 2019 International Conference on Learning Representations*, 121–143, (ICLR, 2019).

47 Kovalenko, K. et al. Vector centrality in hypergraphs. *Chaos Solitons Fractals* **162**, 112397 (2022).

48 Michel, G., Nikolentzos, G., Lutzeyer, J. & Vazirgiannis, M. Path neural networks: expressive and accurate graph neural networks. in *Proc. Int. Conf. Mach. Learn.* 24737–24755 (PMLR, 2023).

49 Zou, C., Lu, G., Du, L., Zeng, X. & Lin, S. Graph similarity learning for cross-level interactions. *Inf. Process. Manag.* **62**, 103932 (2025).

50 Cai, L., Li, J., Wang, J. & Ji, S. Line Graph Neural Networks for Link Prediction. *IEEE Trans. Pattern Anal. Mach. Intell.* **44**, 5103–5113 (2022).

51 Liang, J., Pu, C., Shu, X., Xia, Y. & Xia, C. Line graph neural networks for link weight prediction. *Physica A* **661**, 130406 (2025).

52 Li, M. et al. Line graph contrastive learning for node classification. *J. King Saud Univ. Comput. Inf. Sci.* **36**, 102011 (2024).

53 Papadimitriou, P., Dasdan, A. & Garcia-Molina, H. Web graph similarity for anomaly detection. *J. Internet Serv. Appl.* **1**, 19–30 (2010).

54 Moore, J. M. et al. Network Spreading from Network Dimension. *Phys. Rev. Lett.* **132**, 237401 (2024).

55 Mou, J. et al. The spindle approximation of network epidemiological modeling. *New J. Phys.* **26**, 043027 (2024).

56 Wang, L. et al. Influential nodes identification based on hierarchical structure. *Chaos Soliton Fract.* **186**, 115227 (2024).

57 Namtirtha, A., Dutta, A., et al. Best influential spreaders identification using network global structural properties. *Sci. Rep.* **1**, 1-15 (2011).

58 Ullah, A. *et al*. Identifying vital nodes from local and global perspectives in complex networks. *Expert. Syst. Appl.* **186**, 115778 (2021).

59 Yang, X. & Xiao, F. An improved gravity model to identify influential nodes in complex networks based on k-shell method. Knowl-based Syst. **227**, 107198 (2021).

60 Wang, W., et al. Unification of theoretical approaches for epidemic spreading on complex networks. *Rep. Prog. Phys.* **80**, 036603 (2017).

61 Schieber, T. A. et al. Diffusion capacity of single and interconnected networks. *Nat. Commun.* **14**, 2217 (2023).

62 Ipsen, M., Alexander, S. M. Evolutionary reconstruction of networks. *Phys. Rev. E* **4**, 046109 (2002).

63 Beiró, M. G., Alvarez-Hamelin, J. I. & Busch, J. R. A low complexity visualization tool that helps to perform complex systems analysis. *New J. Phys.* **10**, 125003 (2008).

64 Kirkpatrick, S., Gelatt, C. D. Jr & Vecchi, M. P. Optimization by simulated annealing. *Science* **220**, 671–680 (1983).

65 Milisav, F., Bazinet, V., Betzel, R. F. & Misic, B. A simulated annealing algorithm for randomizing weighted networks. *Nat. Comput. Sci.* **5**, 48–64 (2025).

66 Zachary, W. W. An Information Flow Model for Conflict and Fission in Small Groups. *Journal of Anthropological Research* **33**, 452-473 (1977).

67 Zhang, X. et al. GSpect: Spectral Filtering for Cross-Scale Graph Classification. *IEEE Trans. Netw. Sci. Eng.* **12**, 547–558 (2025).

68 Rousseeuw, P. J. Silhouettes: A graphical aid to the interpretation and validation of cluster analysis. *J Comput Appl Math.* **20**, 53-65 (1987).

69 Matamalas, J. T., Arenas, A. & Gómez, S. Effective approach to epidemic containment using link equations in complex networks. *Sci. Adv.* **4**, eaau4212 (2018).
70 Qin, J.-J. & Yan, G. High Reconstructability of Degree-Heterogeneous Networks. *Phys. Rev. Lett.* **134**, 137402 (2025).
71 Lacasa, L. & Gómez-Gardeñes, J. Correlation Dimension of Complex Networks. *Phys. Rev. Lett.* **110**, 168703 (2013).
72 Moore, J. M. et al. Correlation dimension in empirical networks. *Phys. Rev. E* **107**, 034310 (2023).
73 Erdős, P., & Rényi, A. On Random Graphs I. *Publ. Math. Debrecen* **6**, 290–297 (1959).
74 Watts, D. J. & Strogatz, S. H. Collective dynamics of 'small-world' networks. *Nature* **393**, 440-442 (1998).
75 Barabasi, A.-L. & Albert, R. Emergence of scaling in random networks. *Science* **286**, 509-512 (1999).
76 Lancichinetti, A., Fortunato, S. & Radicchi, F. Benchmark graphs for testing community detection algorithms. *Phys. Rev. E* **78**, 046110 (2008).
77 Tan, S. *et al.* Mobility in China, 2020: a tale of four phases. *Natl. Sci. Rev.* **8**, nwab148 (2021).
78 Dobson, P. D. & Doig, A. J. Distinguishing enzyme structures from non-enzymes without alignments. *J. Mol. Biol.* **330**, 771-783 (2003).
79 Dai, B.-T. *et al.* Measuring the impact of COVID-19 on China's population migration with mobile phone data. *Acta Physica Sinica* **70**, 068901-068910, (2021).

Acknowledgments

This work was supported by the National Natural Science Foundation of China (72025405, 72421002, 92467302, 72088101, 72301285, 72474223), Natural Science Foundation of Hunan Province (2024RC3133, 2023JJ40685), National Key R&D Program of China (2022YFB3102600), the National University of Defense Technology Cornerstone Project (JS24-04), the "Three-Three-Three Project" of Jiangsu Province's High-Level Talent Training Program, and the Startup Foundation for Introducing Talent of NUIST.

Author Contributions

J.M., S.T., and W.L. designed the experiments. J.M., L.W., and C.Z. collected and analyzed data. J.M., L.W., and W.L. interpreted the results. J.M., S.T., and X.L. wrote the manuscript. X.L., B.Z., and S.T. edited and revised the manuscript.

Competing interests

All other authors declare no competing interests.

Figure legends

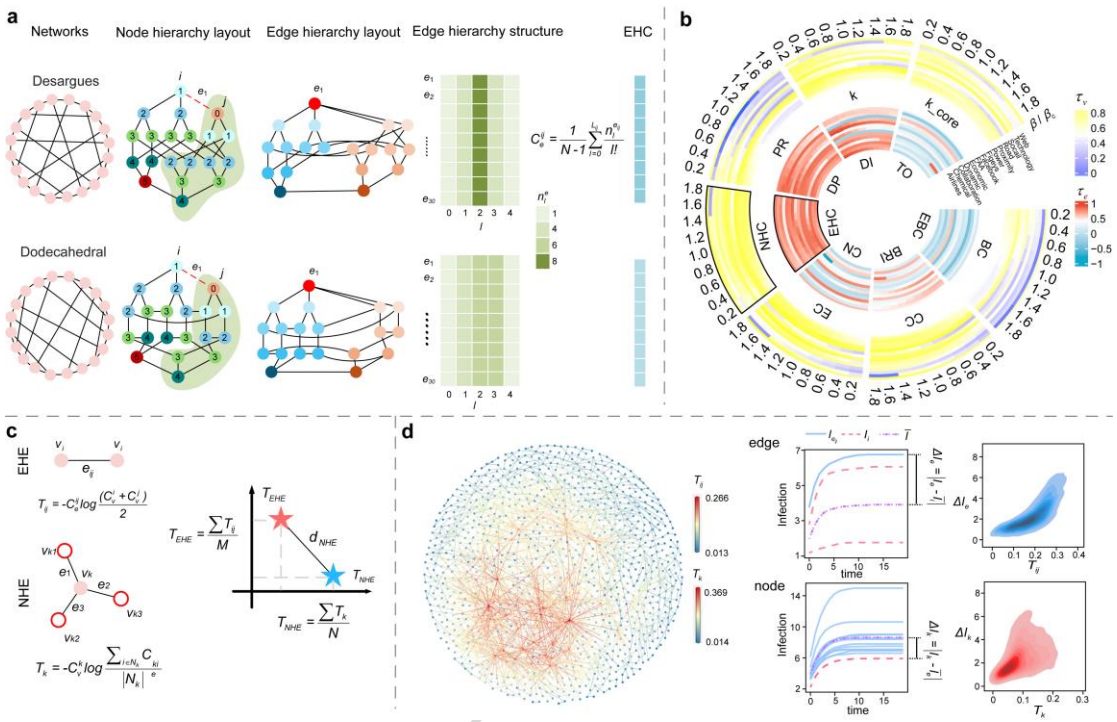

Fig. 1: Overview of the hierarchy entropy-based network dissimilarity metric. Network Hierarchy Entropy (NHE) effectively captures the spreading influence and quantifies the infection gain achieved by simultaneously infecting its connected neighbors, compared to the scenario of infecting only the node itself. **(a)** exemplifies the advantages of node pair shrinking in distinguishing non-isomorphic networks with identical node hierarchy structures, specifically the Desargues and Dodecahedral graphs. The second column illustrates networks structured according to the node hierarchy layout of node *i*, where the layer of nodes originating from node *j* is marked using integers, and the shadow highlights nodes that are one step closer to node *j* than to node *i*. The third column presents the transformed networks after node pair shrinking, according to the edge hierarchy layout of e_1. In this layout, nodes are categorized based on their distances to node *i* (blue) and node *j* (pink). **(b)** highlights the superior performance of node hierarchy centrality (NHC) and edge hierarchy centrality (EHC) in identifying key spreaders across varying infection rate β/β_c compared to degree (*k*), PageRank (PR), betweenness centrality (BC), closeness centrality (CC), eigenvector centrality (EC) and *k*-core for nodes, as well as edge betweenness (EBC), degree product (DP), topological overlap (TO), common neighbors (CN), bridgeness (BRI), and diffusion importance (DI) for edges. The comparison is quantified using Kendall's τ correlations between each centrality and the spreading influence of nodes (τ_v) and edges (τ_e), measured by the average number of infections over 1,000 SIR simulations conducted on 14 networks. **(c)** outlines the definition of network hierarchy entropy and the derived network dissimilarity metric. **(d)** illustrates the spatial distribution and functional significance of hierarchy entropy in the Faa network. Edge hierarchy entropy (T_{ij}) exhibits a strong positive correlation with the edge infection gain ΔI_e, defined as $\Delta I_e = |I_e - \overline{I}_\iota|$ where I_e is the outbreak size from simultaneously infecting both endpoints of an edge, and $\overline{I}_\iota$ is the mean outbreak size from infecting each endpoint individually. Similarly, node hierarchy entropy (T_k) is strongly associated

with its node infection gain ΔI_k, denoted as $\Delta I_k = |\overline{I_e} - I_k|$ where I_k is the outbreak size from infecting the central node, and $\overline{I_e}$ is the mean outbreak size from simultaneously infecting each of its direct neighbors.

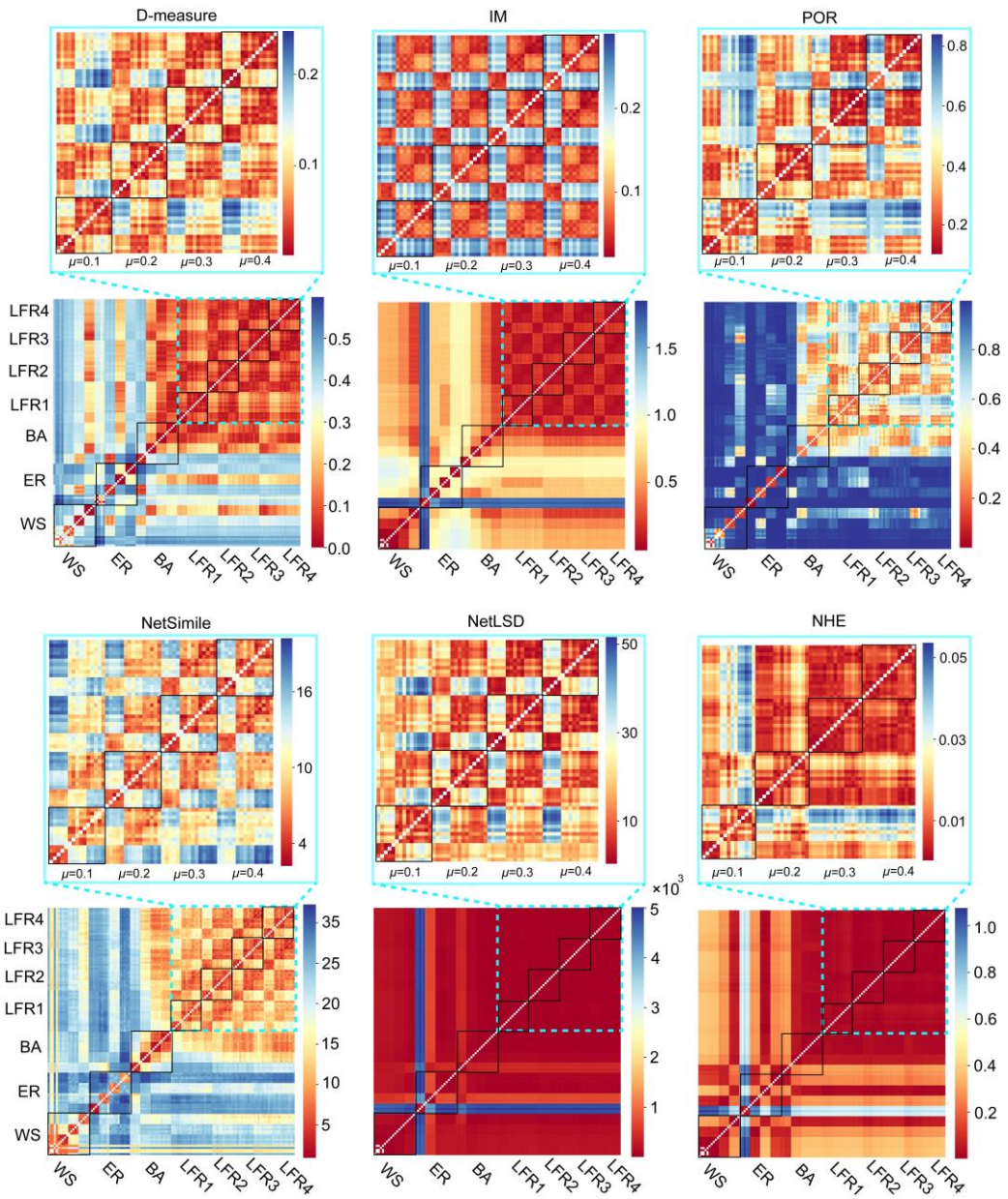

Fig. 2: Structural dissimilarity among synthetic networks. The dissimilarity matrix captures structural differences across Watts-Strogatz (WS), Erdős-Rényi (ER), Barabási–Albert (BA), and Lancichinetti-Fortunato-Radicchi (LFR) networks generated over a range of parameter settings, as detailed in Supplementary Table S3, with five network realizations per parameter set. NHE successfully identifies key evolutionary processes (e.g., WS small-world transition, ER percolation) and discriminates between networks based on community structure strength (μ) in LFR benchmarks. The distance heatmaps in the insets illustrate the dissimilarity between LFR networks grouped by their mixing parameter, including LFR1 (μ=0.1), LFR2 (μ=0.2), LFR3 (μ=0.3), and LFR4 (μ=0.4). For each group, networks were generated with degree distribution exponents λ=1.5, 2.5, and 3.5. Color bars represent the structural dissimilarity as measured by various methods. Distance values of zero are masked to enhance visual clarity.

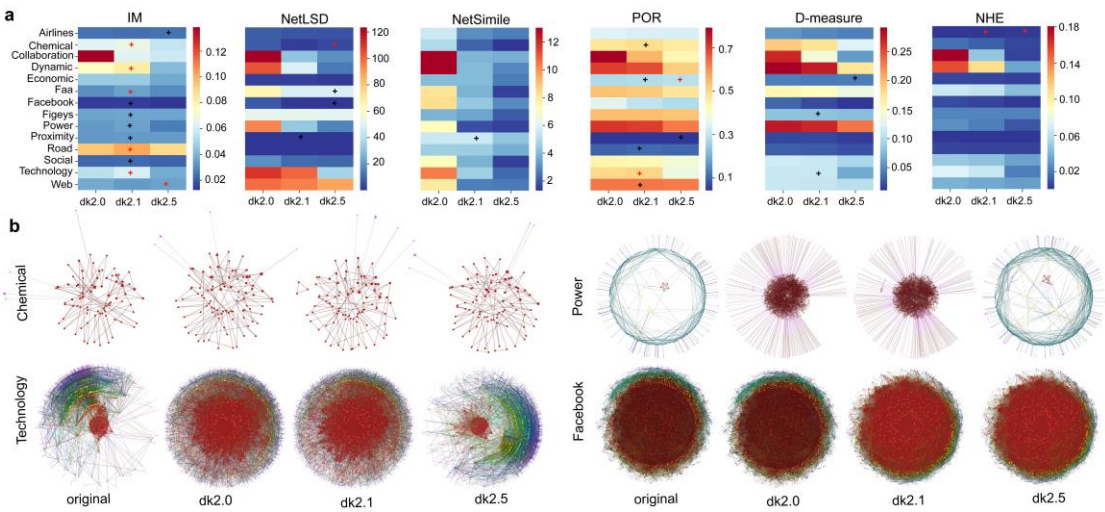

Fig. 3: Comparison among networks generated by dk series models. (a) quantifies the average structural distance over 50 realizations between original networks and their dk series networks. Color bars represent the structural distance as measured by various methods. A "+" symbol represents a violation of the expected dk-series hierarchy, i.e., instances where the distance to a higher-*k* network (e.g., dk2.1 or dk2.5) is greater than the distance to a lower-*k* network (e.g., dk2.0 or dk2.1). A red "+" symbol denotes a significant violation ($p < 0.05$, pairwise t-test). **(b)** visualizes the topological differences between real networks and their dk versions using LaNet-vi. In these visualizations, node sizes are proportional to the logarithm of their degrees, while node color reflects coreness. As *k* increases, dk-random graphs progressively resemble the original networks.

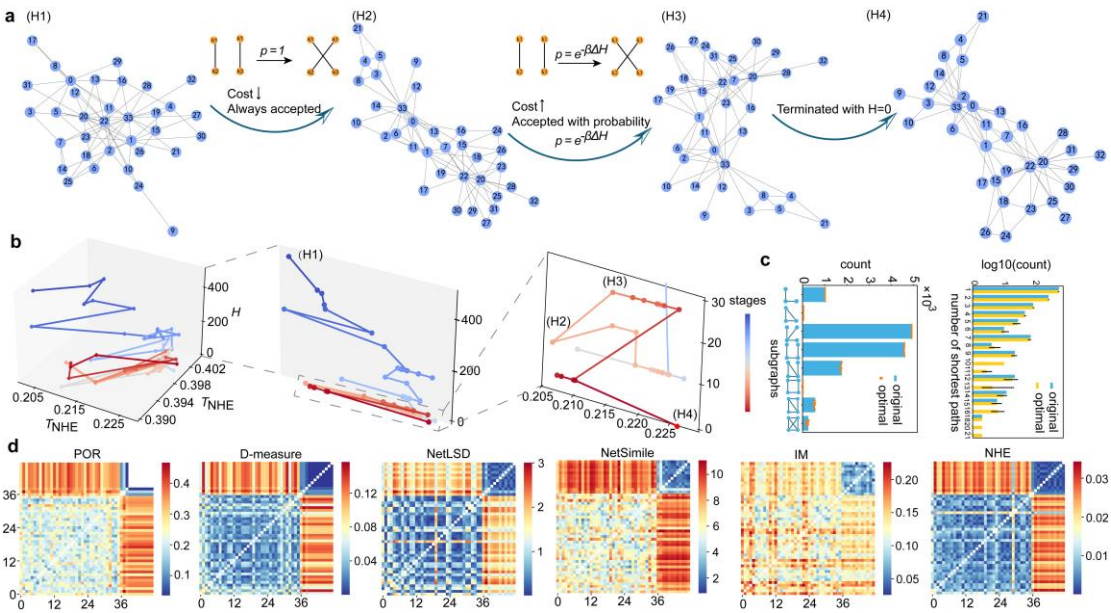

Fig. 4: Performance in comparing networks preserving node hierarchy structure. NHE-based measure demonstrates effectiveness in detecting high-order dissimilarities in empirical networks. **(a)** provides an overview of the simulated annealing algorithm used to search for network assemblies that preserve the node hierarchy structure in the Karate network. The algorithm begins by initializing networks that preserve the degree distribution, followed by iterative edge rewiring with a probability $p = min(1, e^{-\Delta H/T})$, where ΔH represents the change in system energy and T is the system temperature. The system energy is defined as a cost function that evaluates the difference in node distance distributions between the original network and its randomized variants. The optimization process terminates when H=0. **(b)** illustrates the search process for the optimal solution, with energies (H1–H4) corresponding to distinct configurations presented in (a). **(c)** showcases the high-order dissimilarities among 9 configurations that preserve the node hierarchy structure of the Karate network, highlighting the nuanced differences captured by NHE. **(d)** compares the performance of NHE against POR, D-measure, NetLSD, NetSimile, and IM methods in distinguishing 39 networks that preserve degree distributions and 9 networks that preserve the node hierarchy structure, demonstrating the superiority of NHE in identifying high-order structural dissimilarities. Distance values of zero are masked to enhance visual clarity.

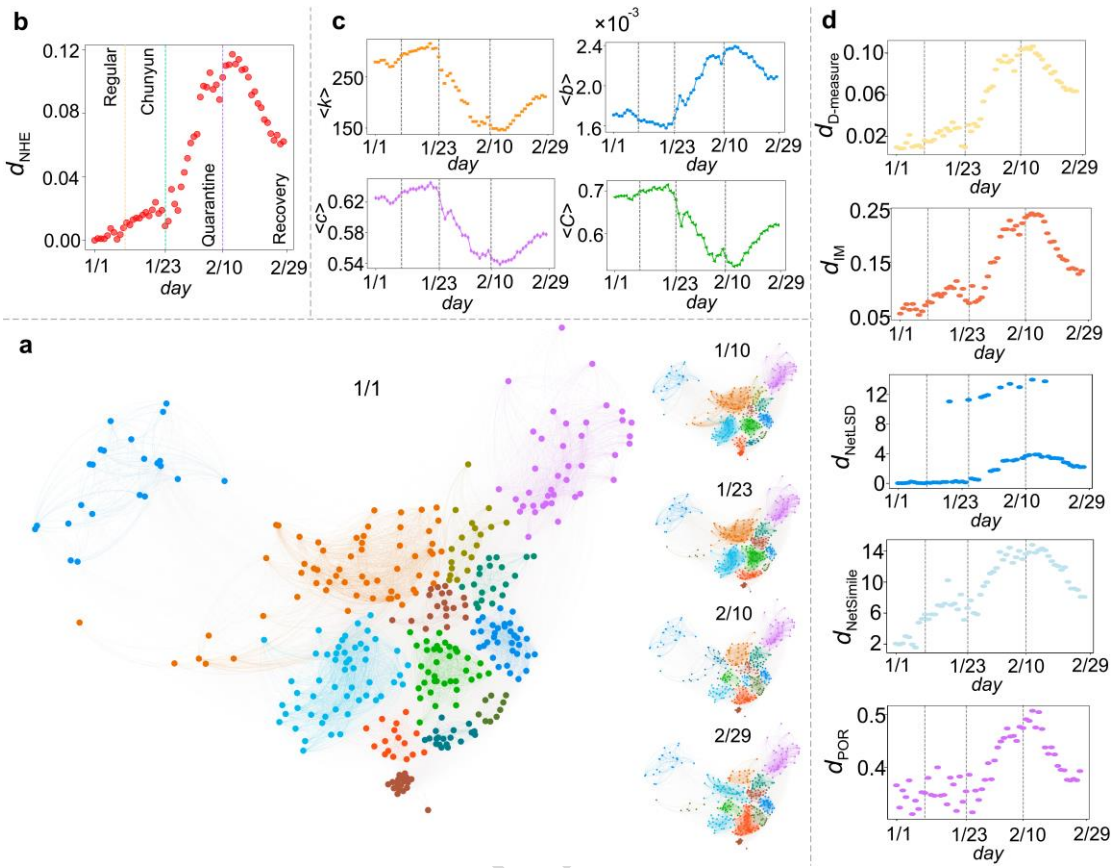

Fig. 5: Evolving pattern characterization for mobility network. NHE provides a more precise characterization of evolving patterns compared to other methods. **(a)** presents snapshots of mobility networks at the beginning of key periods: normal mobility (January 1st), Chunyun (January 10th), quarantine (January 23rd), mobility recovery (February 10th), and the end of February (February 29th). Communities were detected using the Spatial-Louvain algorithm[79], which incorporates both topological connectivity and spatial features via a gravity attenuation factor. Distinct colors represent unique spatial clusters, each consisting of densely interconnected nodes. **(b)** illustrates the evolving pattern of the mobility network, as captured by the structural distance measured by NHE (d_{NHE}) between successive network snapshots and the reference network recorded on January 1st. **(c)** shows the temporal changes in topological features, including the average degree (<*k*>), average betweenness (<*b*>), average closeness (<*c*>), and average clustering coefficient (<*C*>). **(d)** demonstrates the performance of competing methods in capturing the evolution of structural dissimilarity, as measured by D-measure ($d_{\mathrm{D\text{-}measure}}$), IM ($d_{\mathrm{IM}}$), NetLSD ($d_{\mathrm{NetLSD}}$), NetSimile ($d_{\mathrm{NetSimile}}$), and POR ($d_{\mathrm{POR}}$), respectively.

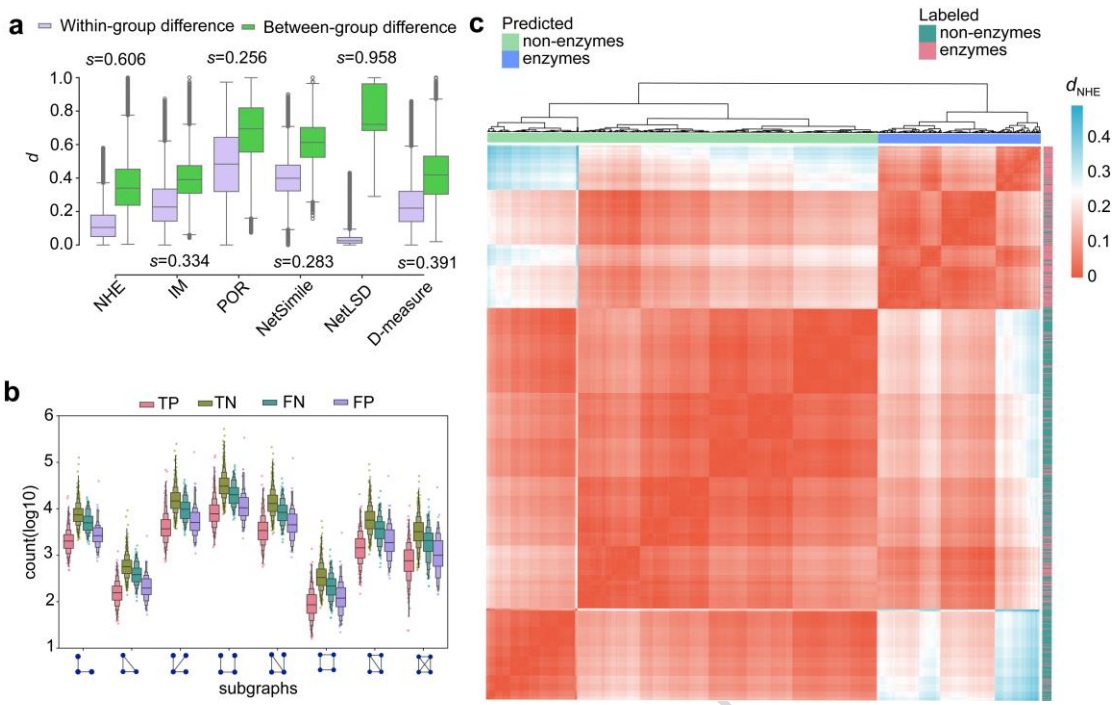

Fig. 6: Distinguishing enzymes from non-enzymes based on network dissimilarity. NHE identifies 346 enzymes, achieving an accuracy of 74.62%. **(a)** shows the within-group and between-group distances for protein clusters using various methods. The Silhouette coefficient (*s*) measures how similar an object is to its own cluster compared to other clusters, involving the mean distance to all other points in the same cluster, and the mean distance to all points in the nearest neighboring cluster. To enable a fair comparison across methods with different scales, all distance metrics are normalized using a Min-Max scaler, for example, $d = (d_{\mathrm{NHE}} - d_{\mathrm{NHE}}^{min})/(d_{\mathrm{NHE}}^{max} - d_{\mathrm{NHE}}^{min})$. NHE exhibits the highest valid clustering efficiency, achieving a Silhouette coefficient of *s*=0.606, outperforming all other methods except NetLSD. However, NetLSD's superior Silhouette score arises from the formation of a small, spurious cluster comprising only two false-positive enzymes. **(b)** illustrates the distribution of subgraphs involving three and four nodes in proteins predicted by NHE. The terms TP (True Positive), FP (False Positive), TN (True Negative), and FN (False Negative) represent the four cases in the classification confusion matrix. The significantly lower counts of three- and four-node subgraphs among predicted enzymes (comprising both TP and FP) compared to predicted non-enzymes (TN and FN) indicate that NHE characterizes enzymes primarily by their reduced participation in these local interaction patterns. **(c)** demonstrates the hierarchy clustering dendrogram with a heatmap of distances measured by NHE (d_{NHE}), where predicted and labeled proteins are colored differently.

Table 1. Classification accuracy of dk-series models based on normalized mutual information

Networks	NHE	IM	POR	NetSimile	NetLSD	D-measure
Chemical	0.610	0.571	0.323	0.650	**0.691**	0.423
Collaboration	**1.000**	**1.000**	**1.000**	0.703	**1.000**	**1.000**
Dynamic	**1.000**	**1.000**	**1.000**	**1.000**	0.900	0.709
Economic	**0.691**	0.652	**0.691**	0.650	0.566	0.181
Facebook	**1.000**	0.118	0.900	**1.000**	0.703	0.709
Power	**1.000**	**1.000**	**1.000**	0.657	0.636	0.669
Proximity	0.147	0.107	0.048	0.181	**0.299**	0.123
Social	**1.000**	0.153	0.658	**1.000**	0.573	0.691
Technology	**1.000**	**1.000**	**1.000**	**1.000**	0.900	0.691
Web	**1.000**	0.506	0.269	0.669	0.691	0.519
Faa	**1.000**	0.538	0.707	**1.000**	0.652	0.707
Figeys	0.643	0.061	0.232	**0.707**	0.086	0.292
Road	0.250	0.138	0.153	0.232	**0.261**	0.100
Airlines	**1.000**	0.088	0.471	**1.000**	0.703	0.359

Note: Normalized Mutual Information (NMI) quantifies the accuracy of cluster assignment across multiple classes. For each case, the highest NMI value is indicated in bold.

Editor Summary-

Quantifying subtle structural differences between networks is challenging, as traditional methods often overlook the interplay between edges and nodes. Here, the authors introduce a dissimilarity measure based on network hierarchy entropy, which captures multiscale structural complexity and achieves high classification accuracy without feature engineering, demonstrating its utility across diverse applications, including evolving pattern analysis and protein classification.

Peer Review Information-

Communications Physics thanks the anonymous reviewers for their contribution to the peer review of this work. A peer review file is available.